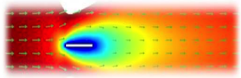
Fenómenos de Transporte

Revista Mexicana de Ingeniería Química

Vol. 13, No. 1 (2014) 259-277

LOW-RAM ALGORITHM FOR SOLVING 3-D NATURAL CONVECTION PROBLEMS USING ORTHOGONAL COLLOCATION

ALGORITMO DE BAJO CONSUMO DE RAM PARA RESOLVER PROBLEMAS DE CONVECCIÓN NATURAL 3-D, USANDO COLOCACIÓN ORTOGONAL

H. Jiménez-Islas[1*], M. Calderón-Ramírez[3], F.I. Molina-Herrera[1], G.M. Martínez-González[2], J.L. Navarrete-Bolaños[1], E.O. Castrejón-González[2]

[1]*Departamento de Ingeniería Bioquímica,* [2] *Departamento de Ingeniería Química,* [3] *Departamento de Ciencias Básicas. Instituto Tecnológico de Celaya. Av. Tecnológico y Antonio García Cubas s/n. Celaya, Guanajuato. C.P.38010. México*

Received May 13, 2013; Accepted January 21, 2014

Abstract

Computational code IMPLI-C3 is a low-RAM consumption program designed to solve three-dimensional parabolic partial differential nonlinear equations. The spatial coordinates are discretized using orthogonal collocation with Legendre polynomials while time was discretized via backward finite differences, generating an implicit method that originates a set of algebraic equations, which are solved by nonlinear relaxation for each step of time integration. Nonlinear relaxation is an iterative method that only uses the Jacobian diagonal and voids the RAM storage of the entire Jacobian matrix. This allows the simulation of physical systems that require greater number of nodes that otherwise would use too much RAM when trying to solve by Newton-Raphson. The code was successfully evaluated using several problems related to natural convection previously reported in literature, observing that nonlinear relaxation only requires 0.3%-1.5% of the memory required by Newton-Raphson for the same problems. Furthermore, one can be conclude that, in problems with many nodes, the use of multivariate Newton-Raphson is unfeasible due to high consumption of RAM that can even cause it to overflow.

Keywords: nonlinear relaxation, natural convection, orthogonal collocation, parabolic partial differential equations.

Resumen

IMPLI-C3 es un código computacional que utiliza bajos recursos de memoria RAM, diseñado para resolver ecuaciones diferenciales parciales parabólicas no lineales en tres dimensiones. Los ejes coordenados en el espacio se discretizaron usando colocación ortogonal con polinomios de Legendre mientras que el tiempo se discretizó mediante diferencias finitas hacia atrás, generando un esquema implícito que origina un conjunto de ecuaciones algebraicas, las cuales se resolvieron mediante relajación no lineal para cada etapa de integración en el tiempo. La relajación no lineal, es un método iterativo que emplea solamente la diagonal del Jacobiano para evitar que se almacene toda la matriz Jacobiana en la memoria RAM de la computadora. Lo anterior permite la simulación de sistemas físicos que requieren mayor cantidad de nodos que, de otra manera emplearían demasiada RAM al intentar resolverlos mediante Newton-Raphson. El código se evaluó satisfactoriamente usando varios problemas relacionados con el fenómeno de convección natural previamente reportados en la literatura, observando que el método de relajación no lineal solamente utiliza entre 0.3% a 1.5% de la memoria con respecto al método de Newton-Raphson. Además se pudo corroborar que, en problemas con muchos nodos, el uso de Newton-Raphson multivariable no es factible debido al consumo elevado de memoria RAM que, inclusive puede provocar su desbordamiento.

Palabras clave: relajación no lineal, convección natural, colocación ortogonal, ecuaciones diferenciales parciales parabólicas.

[*]*Corresponding author. E-mail*: hugo.jimenez@itcelaya.edu.mx
Tel. +52 (461) 611-75-75

1 Introduction

Many problems in the field of Chemical Engineering are modeled as nonlinear partial parabolic differential equations (PDE). Most have only numerical solutions. There are several commercial programs uniquely designed to solve PDE in specific situations, decreasing the versatility of these software. These programs mainly use finite difference or finite element methods, requiring very fine mesh to solve highly nonlinear problems. Therefore, the primary reason to develop a computer code is to increase versatility, especially for highly nonlinear parabolic PDE 3-D problems.

The choice of orthogonal collocation as discretization method is based on its greater precision compared to other well-known methods, such as finite difference. Orthogonal collocation gives smaller margins of error in solutions with the same mesh than other methods (Jiménez-Islas and López-Isunza, 1996; Ebrahimi *et al*., 2008). Villadsen and Stewart (1967) reported several problems focused on chemical engineering, proposing the application of orthogonal collocation to solve differential equations with boundary values. Subsequently, other authors began to expand its use (Ebrahimi *et al*., 2008; Finlayson, 1972; Jiménez-Islas and López-Isunza, 1994; Jiménez-Islas, 2001; Barrozo *et al*., 2006).

The objective of this study is to design an all-purpose computer program that is able to solve in three spatial dimensions any system of nonlinear parabolic PDE 3-D that is presented in dynamic simulation of processes using the orthogonal collocation method for the discretization of the spatial coordinates (Villadsen and Stewart, 1967; Finlayson, 1980; Jiménez-Islas and López-Isunza, 1994) and backward finite differences of the time variable. With the application of the implicit method, a set of nonlinear algebraic equations was obtained. These equations then are solved with nonlinear relaxation (Vemuri and Karplus, 1981) and do not require a special reordering of the governing equations to solve them, unlike other existing solution methods that require specific algebraic arrangements that can be difficult to implement in nonlinear cases. Furthermore, the use of nonlinear relaxation does not require larger RAM such as Newton-based methods, and it is easy to code in any computer language, since operations between vectors are used, while in Newton methods matrix operations are required.

2 Methodology

The basis of the approximation of differential operators via orthogonal collocation requires that the points or nodes correspond to roots of orthogonal polynomials when the residue is zero, Legendre, Jacobi, Hermite, Laguerre, etc. In this work, we used Jacobi polynomials, presented in equation (1). If the coefficients $\alpha = \beta = 0$, equation (1) reduces the orthogonal polynomial to Legendre type.

$$\int_0^1 x^{\alpha}(1-x)^{\beta}P_j(x)P_N(x)dx = 0 \tag{1}$$

In a 2-D domain, the approximation of the solution has the following form:

$$T_{ij} = \sum_{k=1}^{NX+2} b_{ik}x_{ij}^{k-1} \tag{2}$$

Developing the first and second derivative, the following equations were obtained:

$$\left(\frac{dT}{dx}\right)_{ij} = \sum_{k=1}^{NX+2} b_{ik}(k-1)x_{ij}^{k-2} \tag{3}$$

$$\left(\frac{d^2T}{dx^2}\right)_{ij} = \sum_{k=1}^{NX+2} b_{ik}(k-1)(k-2)x_{ij}^{k-3} \tag{4}$$

Where x_{ij} represents the nodes of collocation defined by the roots of orthogonal polynomials used, that represent the points where approximation of differential operators is performed. Generalizing the above equations over the entire domain, we obtained the following equations in matrix notation (Finlayson, 1972, 1980; Jiménez-Islas and López-Isunza, 1994).

$$\mathbf{T} = \mathbf{Q}\mathbf{b} \tag{5}$$

$$\frac{\mathrm{d}\mathbf{T}}{\mathrm{dx}} = \mathbf{C}\mathbf{b} \tag{6}$$

$$\frac{\mathrm{d}^2\mathbf{T}}{\mathrm{dx}^2} = \mathbf{D}\mathbf{b} \tag{7}$$

Where

$$Q_{ik} = x_{ii}^{k-1} \tag{8}$$

$$C_{ik} = (k-1)x_{ii}^{k-2} \tag{9}$$

$$D_{ik} = (k-1)(k-2)x_{ii}^{k-3} \tag{10}$$

Solving for **b** gives the following:

$$\mathbf{b} = \mathbf{Q}^{-1}\mathbf{T} \tag{11}$$

Substituting the expression (11) in (6) and (7) yields the following:

$$\frac{\mathrm{d}\mathbf{T}}{\mathrm{dx}} = \mathbf{C}\mathbf{Q}^{-1}\mathbf{T} = \mathbf{A}\mathbf{T} \tag{12}$$

$$\frac{\mathrm{d}^2\mathbf{T}}{\mathrm{dx}^2} = \mathbf{D}\mathbf{Q}^{-1}\mathbf{T} = \mathbf{B}\mathbf{T} \tag{13}$$

Where **A** and **B** are the collocation matrices that approximate the first and second derivative, respectively. Expanding these definitions to three spatial coordinates gives the following equations (Jiménez-Islas, 2001):

$$\frac{\partial T}{\partial x} = \sum_{p=1}^{NX+2} AX_{ip}T_{pjk} \tag{14}$$

$$\frac{\partial^2 T}{\partial x^2} = \sum_{p=1}^{NX+2} BX_{ip}T_{pjk} \tag{15}$$

$$\frac{\partial T}{\partial y} = \sum_{p=1}^{NY+2} AY_{jp}T_{ipk} \tag{16}$$

$$\frac{\partial^2 T}{\partial y^2} = \sum_{p=1}^{NY+2} BY_{jp}T_{ipk} \tag{17}$$

$$\frac{\partial T}{\partial z} = \sum_{p=1}^{NZ+2} AZ_{kp}T_{ijp} \tag{18}$$

$$\frac{\partial^2 T}{\partial z^2} = \sum_{p=1}^{NZ+2} BZ_{kp}T_{ijp} \tag{19}$$

The orthogonal collocation method includes all nodes present in the discretization of partial derivatives and generates greater accuracy with smaller meshes than finite differences (Jiménez-Islas, 1999; Jiménez-Islas, 2001). By using a finite backward difference in time, which produces a system of nonlinear algebraic equations that resolves simultaneously for each integration step. The implicit method is unconditionally stable and less dependent on the size of stages that occur in explicit methods (Vemuri and Karplus, 1981). The numerical solution of systems in three dimensions using orthogonal collocation requires the generation of a large matrix that increases geometrically with the number of nodes. It is necessary to find a method that does not require the RAM storage of the Jacobian matrix of Newton-Raphson method. Nonlinear relaxation is one of the alternative methods, which consists of applying a one-dimensional Newton-Raphson to each equation to achieve convergence. Therefore, we only use the diagonal of the Jacobian matrix (Vemuri and Karplus, 1981). Equation (20) shows a relaxation scheme in a nonlinear variant, where λ is a relaxation factor that accelerates and achieves convergence, and determines the dimensional displacement of the solution.

$$x_i^{k+1} = x_i^k - \lambda \frac{f_i\left(x_1^{k+1}, x_2^{k+1}, \ldots, x_i^k, \ldots, x_n^k\right)}{\frac{\partial f_i}{\partial x_i}\Big|\left(x_1^{k+1}, x_2^{k+1}, \ldots, x_i^k, \ldots, x_n^k\right)} \tag{20}$$

The convergence ratio of nonlinear relaxation depends of the initial value of λ and, in higher nonlinear problems, requires commonly many iterations to achieve the fixed tolerance. However, the iterations run quickly and are easy to code for parallel platforms. Typically, one can propose an initial value of $\lambda = 0.5$ for exploring convergence. Taking the considerations discussed above, we developed a program coded in FORTRAN 90 called IMPLI-C3. This computational code can be used interchangeably on x86 platforms, workstations and supercomputers (using parallel processing). In addition, we developed an easy notation for feeding PDE and their boundaries and initial conditions in an IMPLI-C3 subroutine. For example: T_1 is $T(1)$, $\frac{\partial T_1}{\partial x}$ is TX(1), $\frac{\partial^2 T_2}{\partial z^2}$ is TZZ(2), etc. This notation was used successfully in other computer codes (Jiménez-Islas, 1999; Jiménez-Islas, 2001; Carrera-Rodríguez *et al*, 2011). For the simulations, we used a midrange computer with microprocessor Intel Core^{TM} 2 Duo E4500, 2.20 GHz with 2 Gb RAM, Windows XP^{TM} and COMPAQ^{TM} Visual FORTRAN compiler v. 6.6c.

To assess the reliability of IMPLI-C3 software, the computer code was validated with four study cases, three of which are related to natural convection. Case I is a designed system of coupled nonlinear parabolic PDE that has an analytical solution and allows us to analyze the error rate via a mesh independence analysis. The remaining cases are associated with natural convection phenomenon defined as heat or mass transport due buoyancy forces. There exists a great diversity of buoyancy flows in enclosures that are of interest in science and technology. These buoyancy flows involve challenging physical and mathematical problems as the coupling of the flow and transport and of the boundary layer and core flows, the interaction between the flow and the driving force, which alters the regions in which the buoyancy acts, and the occurrence of multicellular flow. (Ostrach, 1988; Nield and Bejan, 1992, Jiménez-Islas, 1999).

The second case enhances the utility of the increment of nodes close the boundaries in a cylindrical geometry problem with asymmetric behavior (Ozoe and Toh, 1998). The third case is

the classical problem of natural convection in a cubical cavity, which is often used as a benchmark for assessing new algorithms or codes (De Vahl Davis, 1983; Bessonov *et al*., 1998; Tric *et al*., 2000; Wakashima and Saitoh, 2004; Ravnik *et al*., 2008; Brahim and Taieb, 2009). The fourth case, which is an application of this code to solve the problem of natural convection in grain storage in cylindrical silos, demonstrates the robustness of IMPLI-C3 in solving complex problems. The convergence criterion is (Carrera-Rodríguez *et al*., 2011) as follows:

$$\left|f_i\left(x_1^{k+1}, x_2^{k+1}, \ldots, x_i^k, \ldots, x_n^k\right)\right| \leq 10^{-5}$$
for all discretized equations (21)

3 Results and discussion

3.1 Case I: A system of two coupled nonlinear PDE with known analytical solution

In this study case, we constructed an arbitrary system of 3-D parabolic PDE with analytical solution, the equations were:

$$\frac{\partial T_1}{\partial t} = \frac{\partial^2 T_1}{\partial X^2} + \frac{\partial^2 T_1}{\partial Y^2} + \frac{\partial^2 T_1}{\partial Z^2} - \frac{\partial T_1}{\partial X}\frac{\partial T_2}{\partial Y} - \frac{\partial T_1}{\partial Y}\frac{\partial T_2}{\partial Z} + T_2 + e^{-t}\left(4Y^3 - Y^2 - Z\right) + 24X^2YZ - X\left(3Z^2 + 4\right) \quad (22a)$$

$$\frac{\partial T_2}{\partial t} = \frac{\partial^2 T_2}{\partial X^2} + \frac{\partial^2 T_2}{\partial Y^2} + \frac{\partial^2 T_2}{\partial Z^2} - T_2\frac{\partial T_1}{\partial X} - T_1\frac{\partial T_2}{\partial Z} + e^{-t}\left(6XZ^2 + 2Y^4 - Y^2 - 2\right) + 12X^2Y^2Z + 6X\left(Y^2Z^2 - 1\right) \quad (22b)$$

With the following boundary and initial conditions:

$$X = 0, \quad T_1 = Ze^{-t}, T_2 = Y^2e^{-t} \quad (23a)$$

$$X = 1, \quad \frac{\partial T_1}{\partial X} = 2Y^2, \frac{\partial T_2}{\partial X} = 3Z^2 \quad (23b)$$

$$Y = 0, \quad T_1 = Ze^{-t}, T_2 = 3XZ^2 \quad (23c)$$

$$Y = 1, \quad \frac{\partial T_1}{\partial Y} = 4X, \frac{\partial T_2}{\partial Y} = 2e^{-t} \quad (23d)$$

$$Z = 0, \quad T_1 = 2XY^2, T_2 = Y^2e^{-t} \quad (23e)$$

$$Z = 1, \quad \frac{\partial T_1}{\partial Z} = e^{-t}, \frac{\partial T_2}{\partial Y} = 6X \quad (23f)$$

$$t = 0, \quad T_1 = 2XY^2 + Z, T_2 = 3XZ^2 + Y^2 \quad (23g)$$

The system was discretized with $7 \times 7 \times 7$, $9 \times 9 \times 9$, $13 \times 13 \times 13$, $15 \times 15 \times 15$, and $21 \times 21 \times 21$ orthogonal collocation internal points with Legendre polynomials and integrated from $t = 0$ to $t = 2$ with 200 steps, a relaxation factor λ of 0.7 and a tolerance of 10^{-5}. We also carried out the calculation of the relative errors of each variable for $t = 2$ and verified the error diminishing and the iterations increasing with increasing the mesh size. These data, shown in Table 1, were compared with the analytic solution of the coupled parabolic PDE: $T_1 = 2XY^2 + Ze^{-t}$ and $T_2 = 3XZ^2 + Y^2e^{-t}$.

Table 1. Analysis of mesh independence in Case I, using the average error of the variables T_1 and T_2

Mesh	Iterations	Error T_1	Error T_2
7×7×7	49143	6.4 %	5.1 %
9×9×9	85078	5.1 %	3.6 %
13×13×13	205671	4.1 %	2.2 %
15×15×15	289312	3.9 %	1.9 %
21×21×21	642630	3.5 %	1.4 %

The simulations were continued with the integration of the system until steady state was reached at $t = 10$ (transient term average value equal to 10^{-5}). Fig. 1 depicts a comparison of isosurfaces of the variables T_1 and T_2, including both the numerical and analytical results, confirming an excellent agreement.

3.2 Case II: Free convection in a cylinder

We have analyzed the 3-D natural convection in a cylinder in which a point of singularity occurs along the axial axis if the problem is modeled using cylindrical coordinates. Ozoe and Toh (1998) have suggested solving the problem using asymmetric boundary conditions so that the values of nodes located in the axial axis are approximated via the average of adjacent nodes. The Navier-Stokes and energy balance equations were solved using Boussinesq approximation (Leonardi, 1984) and Vector Potential-Vorticity (VP-V) formulation, where the pressure and the velocity fields were become to a new expression known as vector potential ψ, which represent a fluid rotational normal vector related to the momentum equations (Roache, 1972) for Pr = 1 and Ra = 10^3 (Ozoe and Toh, 1998).

Potential Vector Equations:

$$\omega_r = -\left(\frac{\partial^2\psi_r}{\partial\xi^2} + \frac{1}{\xi}\frac{\partial\psi_r}{\partial\xi} - \frac{\psi_r}{\xi^2} + \frac{1}{4\pi^2\xi^2}\frac{\partial^2\psi_r}{\partial\eta^2} - \frac{2}{4\pi^2\xi^2}\frac{\partial\psi_\theta}{\partial\eta} + \frac{1}{\mathrm{A}^2}\frac{\partial^2\psi_r}{\partial\zeta^2}\right) \tag{24a}$$

$$\omega_\theta = -\left(\frac{\partial^2\psi_\theta}{\partial\xi^2} + \frac{1}{\xi}\frac{\partial\psi_\theta}{\partial\xi} - \frac{\psi_\theta}{\xi^2} + \frac{1}{\xi^2}\frac{\partial^2\psi_\theta}{4\pi^2\partial\eta^2} + \frac{2}{\xi^2}\frac{\partial\psi_r}{\partial\eta} + \frac{1}{\mathrm{A}^2}\frac{\partial^2\psi_\theta}{\partial\zeta^2}\right) \tag{24b}$$

$$\omega_z = -\left(\frac{\partial^2\psi_z}{\partial\xi^2} + \frac{1}{\xi}\frac{\partial\psi_z}{\partial\xi} + \frac{1}{\xi^2}\frac{\partial^2\psi_z}{4\pi^2\partial\eta^2} + \frac{1}{\mathrm{A}^2}\frac{\partial^2\psi_z}{\partial\zeta^2}\right) \tag{24c}$$

Vorticity Equations:

$$\begin{aligned}\frac{\partial\omega_r}{\partial\mathrm{Fo}} = &\left[\begin{array}{l}\left[\begin{array}{l}\omega_r\left(\frac{1}{4\pi^2\xi}\frac{\partial^2\psi_z}{\partial\xi\partial\eta} - \frac{1}{4\pi^2\xi^2}\frac{\partial\psi_z}{\partial\eta} - \frac{1}{A^2}\frac{\partial^2\psi_\theta}{\partial\xi\partial\zeta}\right) + \omega_\theta\left(\begin{array}{l}\frac{1}{16\pi^4\xi^2}\frac{\partial^2\psi_z}{\partial\eta^2} - \frac{1}{4\pi^2\xi A^2}\frac{\partial\psi_\theta}{\partial\eta\partial\zeta}\\ +\frac{1}{4\pi^2\xi}\frac{\partial\psi_z}{\partial\xi} - \frac{1}{4\pi^2\xi A^2}\frac{\partial\psi_r}{\partial\zeta}\end{array}\right)\\ +\omega_z\left(\frac{1}{4\pi^2\xi\mathrm{A}^2}\frac{\partial^2\psi_z}{\partial\zeta\partial\eta} - \frac{1}{\mathrm{A}^4}\frac{\partial^2\psi_\theta}{\partial\zeta^2}\right)\end{array}\right]\\ -\left[\begin{array}{l}\left(\frac{1}{4\pi^2\xi}\frac{\partial\psi_z}{\partial\eta} - \frac{1}{\mathrm{A}^2}\frac{\partial\psi_\theta}{\partial\zeta}\right)\left(\frac{\partial\omega_r}{\partial\xi}\right) + \left(-\frac{\partial\psi_z}{\partial\xi} + \frac{1}{\mathrm{A}^2}\frac{\partial\psi_r}{\partial\zeta}\right)\left(\frac{1}{4\pi^2\xi}\frac{\partial\omega_r}{\partial\eta} - \frac{\omega_\theta}{4\pi^2\xi}\right)\\ +\left(\frac{\partial\psi_\theta}{\partial\xi} + \frac{\psi_\theta}{\xi} - \frac{1}{4\pi^2\xi}\frac{\partial\psi_r}{\partial\eta}\right)\left(\frac{1}{\mathrm{A}^2}\frac{\partial\omega_r}{\partial\zeta}\right)\end{array}\right]\end{array}\right]\\ &+\mathrm{Pr}\left(\frac{\partial^2\omega_r}{\partial\xi^2} + \frac{1}{\xi}\frac{\partial\omega_r}{\partial\xi} - \frac{\omega_r}{\xi^2} + \frac{1}{4\pi^2\xi^2}\frac{\partial^2\omega_r}{\partial\eta^2} - \frac{2}{4\pi^2\xi^2}\frac{\partial\omega_\theta}{\partial\eta} + \frac{1}{A^2}\frac{\partial^2\omega_r}{\partial\zeta^2}\right) + \mathrm{RaPrA}\left(\frac{1}{4\pi^2\xi}\frac{\partial\theta}{\partial\eta}\right)\end{aligned} \tag{24d}$$

$$\begin{aligned}\frac{\partial\omega_\theta}{\partial\mathrm{Fo}} = &\left[\begin{array}{l}\left[\begin{array}{l}\omega_r\left(\frac{1}{A^2}\frac{\partial\psi_r}{\partial\xi\partial\zeta} - \frac{\partial^2\psi_z}{\partial\xi^2}\right) + \omega_\theta\left(\begin{array}{l}\frac{1}{4\pi^2\xi\mathrm{A}^2}\frac{\partial^2\psi_r}{\partial\eta\,\partial\zeta} - \frac{1}{\xi\mathrm{A}^2}\frac{\partial\psi_\theta}{\partial\zeta}\\ -\frac{1}{4\pi^2\xi}\frac{\partial^2\psi_z}{\partial\eta\,\partial\xi} + \frac{1}{4\pi^2\xi^2}\frac{\partial\psi_z}{\partial\eta}\end{array}\right)\\ +\omega_z\left(\frac{1}{A^4}\frac{\partial^2\psi_r}{\partial\zeta^2} - \frac{1}{\mathrm{A}^2}\frac{\partial^2\psi_z}{\partial\xi\,\partial\zeta}\right)\end{array}\right]\\ -\left[\begin{array}{l}\left(\frac{1}{4\pi^2\xi}\frac{\partial\psi_z}{\partial\eta} - \frac{1}{A^2}\frac{\partial\psi_\theta}{\partial\zeta}\right)\left(\frac{\partial\omega_\theta}{\partial\xi}\right) + \left(-\frac{\partial\psi_z}{\partial\xi} + \frac{1}{\mathrm{A}^2}\frac{\partial\psi_r}{\partial\zeta}\right)\left(\frac{1}{4\pi^2\xi}\frac{\partial\omega_\theta}{\partial\eta} + \frac{\omega_r}{\xi}\right)\\ +\left(\frac{\partial\psi_\theta}{\partial\xi} + \frac{\psi_\theta}{\xi} - \frac{1}{4\pi^2\xi}\frac{\partial\psi_r}{\partial\eta}\right)\left(\frac{1}{\mathrm{A}^2}\frac{\partial\omega_\theta}{\partial\zeta}\right)\end{array}\right]\end{array}\right]\\ &+\mathrm{Pr}\left(\frac{\partial^2\omega_\theta}{\partial\xi^2} + \frac{1}{\xi}\frac{\partial\omega_\theta}{\partial\xi} - \frac{\omega_\theta}{\xi^2} + \frac{1}{\xi^2}\frac{\partial^2\omega_\theta}{4\pi^2\partial\eta^2} + \frac{2}{\xi^2}\frac{\partial\omega_r}{\partial\eta} + \frac{1}{\mathrm{A}^2}\frac{\partial^2\omega_\theta}{\partial\zeta^2}\right) - \mathrm{RaPrA}\left(\frac{\partial\theta}{\partial\xi}\right)\end{aligned} \tag{24e}$$

$$\frac{\partial \omega_z}{\partial \mathrm{Fo}} = \left[\begin{array}{l} \left[\begin{array}{l} \omega_r\left(\frac{1}{\xi}\frac{\partial \psi_\theta}{\partial \xi} - \frac{\psi_\theta}{\xi^2} + \frac{\partial^2 \psi_\theta}{\partial \xi^2} - \frac{1}{4\pi^2\xi}\frac{\partial^2 \psi_r}{\partial \xi \partial \eta} + \frac{1}{4\pi^2\xi^2}\frac{\partial \psi_r}{\partial \eta}\right) + \omega_\theta\left(\frac{1}{4\pi^2\xi^2}\frac{\partial \psi_\theta}{\partial \eta} + \frac{1}{4\pi^2\xi}\frac{\partial^2 \psi_\theta}{\partial \xi \partial \eta} - \frac{1}{16\pi^4\xi^2}\frac{\partial^2 \psi_r}{\partial \eta^2}\right) \\ +\omega_z\left(\frac{1}{\mathrm{A}^2\xi}\frac{\partial \psi_\theta}{\partial \zeta} + \frac{1}{\mathrm{A}^2}\frac{\partial^2 \psi_\theta}{\partial \xi \partial \zeta} - \frac{1}{4\pi^2\xi\mathrm{A}^2}\frac{\partial^2 \psi_r}{\partial \eta \partial \zeta}\right) \end{array}\right] \\ -\left[\begin{array}{l} \left(\frac{1}{4\pi^2\xi}\frac{\partial \psi_z}{\partial \eta} - \frac{1}{\mathrm{A}^2}\frac{\partial \psi_\theta}{\partial \zeta}\right)\left(\frac{\partial \omega_z}{\partial \xi}\right) + \left(-\frac{\partial \psi_z}{\partial \xi} + \frac{1}{\mathrm{A}^2}\frac{\partial \psi_r}{\partial \zeta}\right)\left(\frac{1}{4\pi^2\xi}\frac{\partial \omega_z}{\partial \eta}\right) \\ +\left(\frac{\partial \psi_\theta}{\partial \xi} + \frac{\psi_\theta}{\xi} - \frac{1}{4\pi^2\xi}\frac{\partial \psi_r}{\partial \eta}\right)\left(\frac{1}{\mathrm{A}^2}\frac{\partial \omega_z}{\partial \zeta}\right) \end{array}\right] \\ +\mathrm{Pr}\left(\frac{\partial^2 \omega_z}{\partial \xi^2} + \frac{1}{\xi}\frac{\partial \omega_z}{\partial \xi} + \frac{1}{\xi^2}\frac{\partial^2 \omega_z}{4\pi^2\partial \eta^2} + \frac{1}{\mathrm{A}^2}\frac{\partial^2 \omega_z}{\partial \zeta^2}\right) \end{array}\right] \tag{24f}$$

Energy Equation:

$$\frac{\partial \theta}{\partial \mathrm{Fo}} = \left(\frac{1}{\mathrm{A}^2}\frac{\partial \psi_\theta}{\partial \zeta} - \frac{1}{4\pi^2\xi}\frac{\partial \psi_z}{\partial \eta}\right)\frac{\partial \theta}{\partial \xi} + \frac{1}{4\pi^2\xi}\left(\frac{\partial \psi_z}{\partial \xi} - \frac{1}{\mathrm{A}^2}\frac{\partial \psi_r}{\partial \zeta}\right)\frac{\partial \theta}{\partial \eta} + \frac{1}{\mathrm{A}^2}\left(\frac{1}{4\pi^2\xi}\frac{\partial \psi_r}{\partial \eta} - \frac{\partial \psi_\theta}{\partial \xi} - \frac{\psi_\theta}{\xi}\right)\frac{\partial \theta}{\partial \zeta} + \frac{\partial^2 \theta}{\partial \xi^2} + \frac{1}{\xi}\frac{\partial \theta}{\partial \xi} + \frac{1}{4\pi^2\xi^2}\frac{\partial^2 \theta}{\partial \eta^2} + \frac{1}{\mathrm{A}^2}\frac{\partial^2 \theta}{\partial \zeta^2} \tag{25}$$

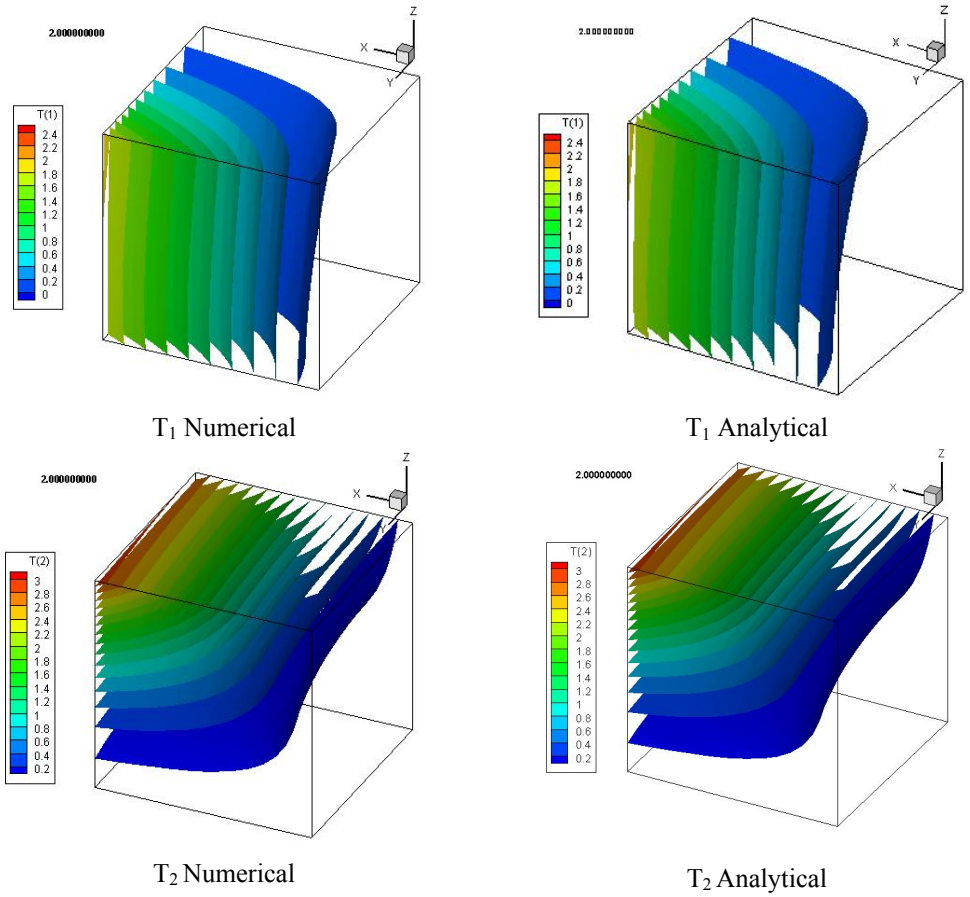

T_1 Numerical T_1 Analytical

T_2 Numerical T_2 Analytical

Fig. 1. Comparison of numerical and analytical isosurfaces T_1 and T_2 at t = 2.0, for Case I.

After dimensionless procedure and the VP-V methodology, appear terms that relate the system characteristics. Rayleigh number (Ra) indicates the relative magnitude of buoyancy driven flow due to differences of temperature and density. Prandtl number (Pr) is the rate of momentum and thermal diffusivities, giving a measurement of the transport hydrodynamic and energy efficiency, and the geometric relation (A) is just as the cavity changes in dimensions.

We have used an average of the node values around the center ($r = 0$) to define the boundary condition in this point (Ozoe and Toh, 1998). The cylinder walls shows no-slip condition for the vector potential, and vorticity is modeled using Wood's approximation (Roache, 1972) ($\xi = 1$, $\zeta = 0$, $\zeta = 1$), and equality in field and flux in the azimuthal coordinate (0 and 2π, respectively). Temperature remained constant at the bottom, top and halfway around the cylinder with sinusoidal variation and was proven for the two cases used by Ozoe and Toh (1998) shown in Fig. 2. The problem was solved using 9 nodes to radial and axial and 15 azimuthally nodes. This gridding was employed to improve the calculation of the azimuthal coordinate. Fig. 3 shows the coordinate system and the mesh grid used in the numerical experiment.

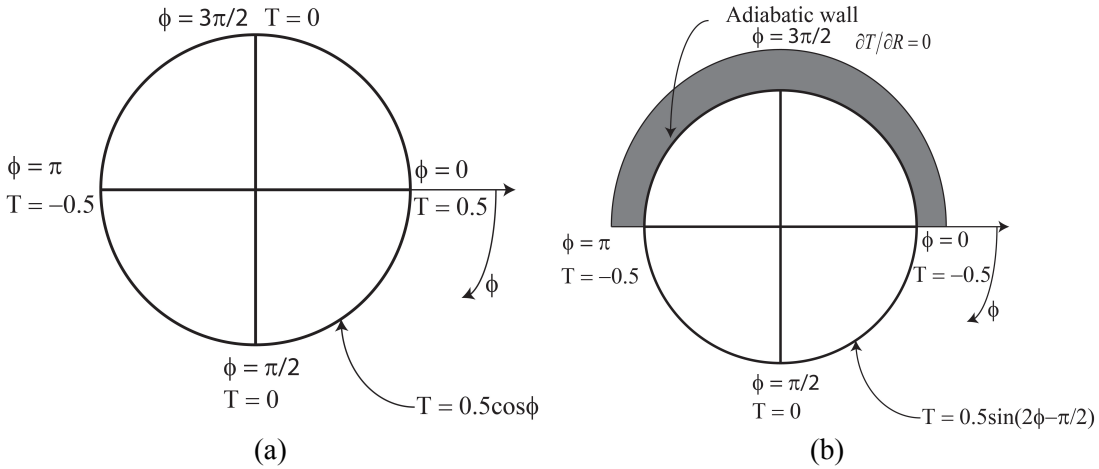

Fig. 2. Temperature boundary conditions used. Top views of the cylinder with thermal boundary conditions for two systems of sample computation: a) model A, b) model B taken from Ozoe and Toh (1998).

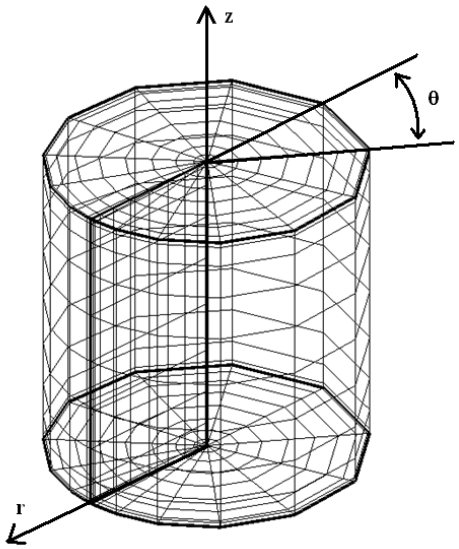

Fig. 3. Cylindrical mesh for sample computations in Case II.

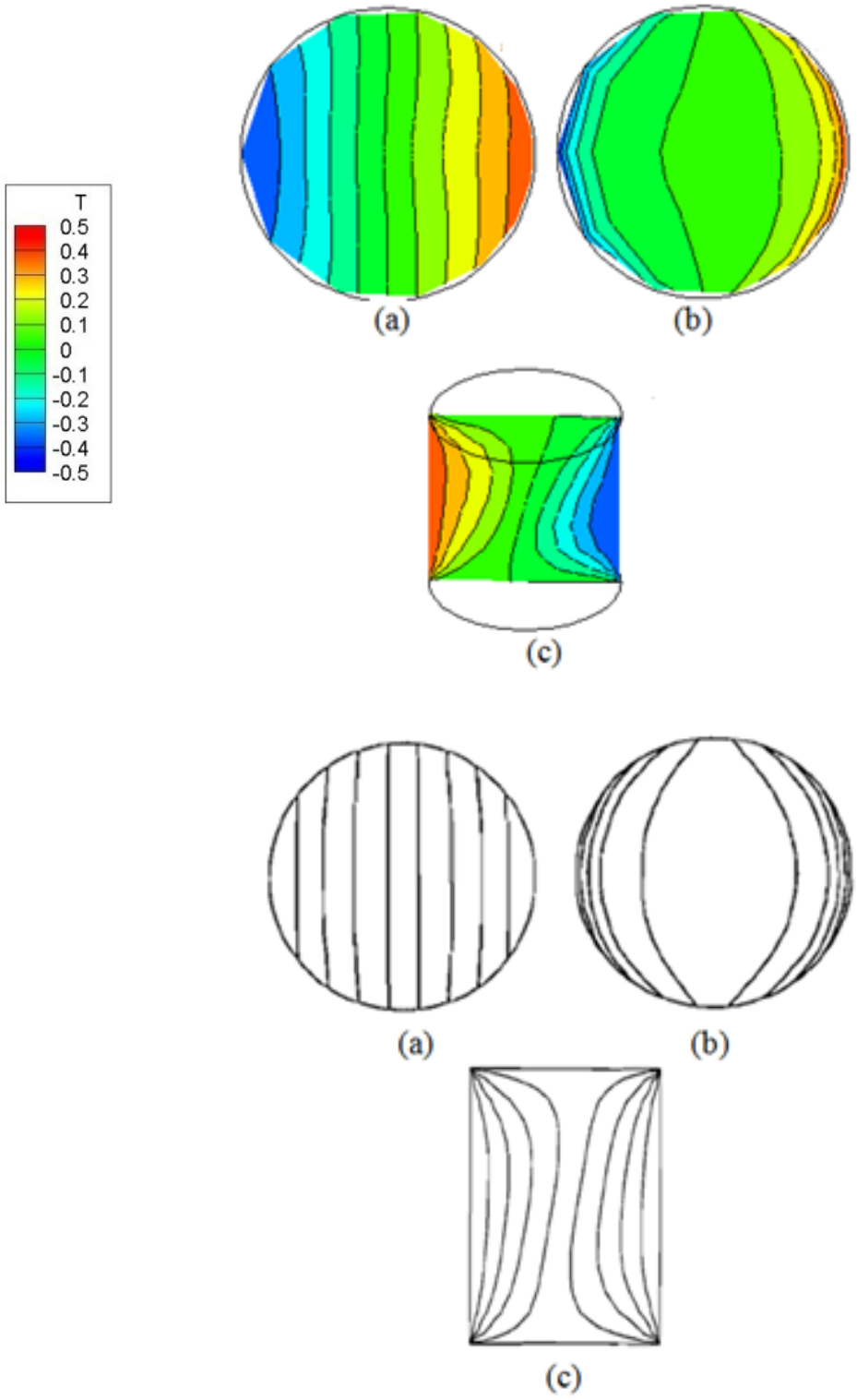

Fig. 4. Comparative case A, Top views of the isotherms at Fo = 0.35, a) ζ= 0.5, b) ζ= 12.5/13, and side view in the vertical plane c) $\theta = 0$ and $\theta = \pi$. The black-line plots were taken from Ozoe and Toh (1998) for comparison purposes.

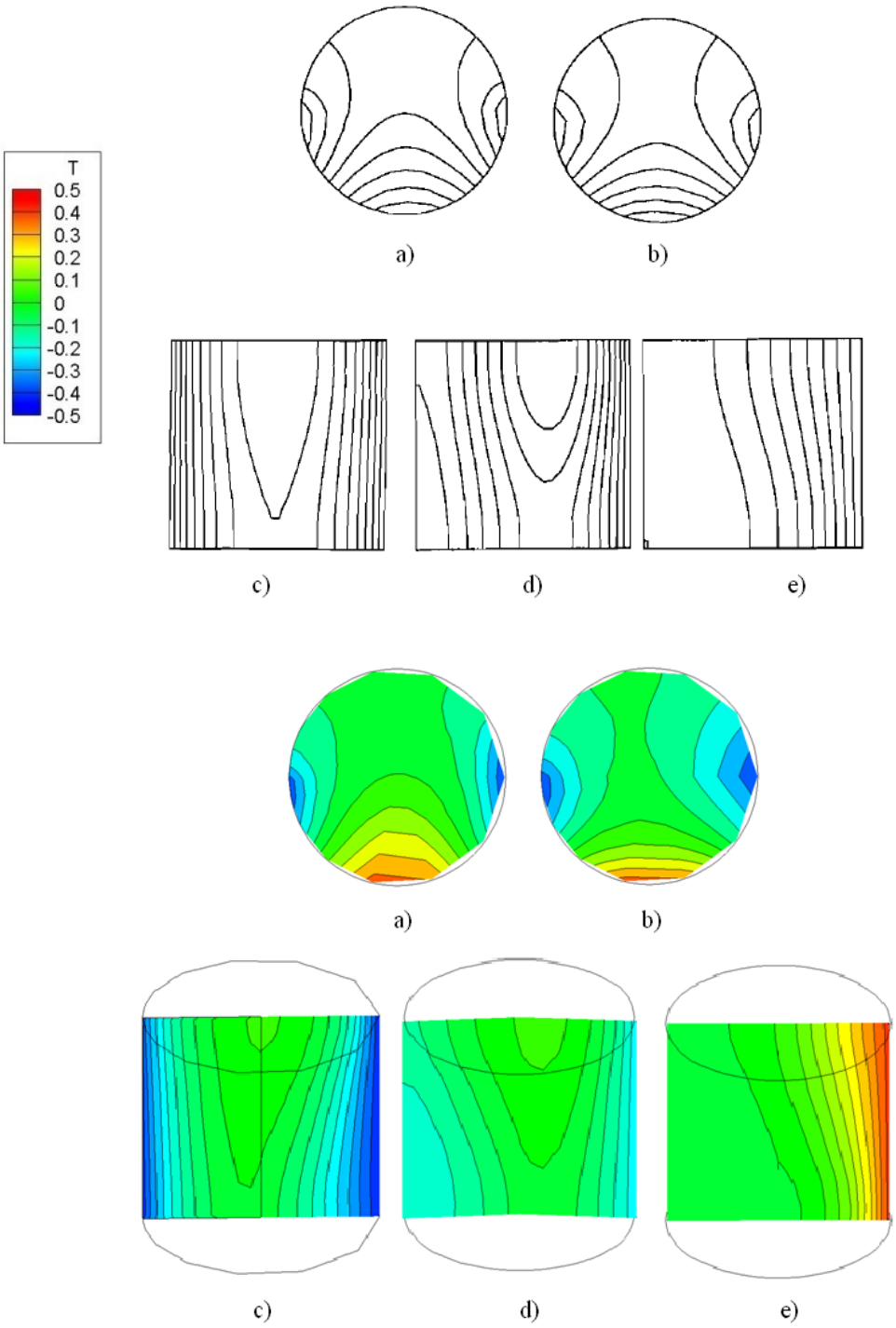

Fig. 5. Comparative case B, Top views of the isotherms at Fo=0.45, a) $\zeta = 0.5/13$ b) $\zeta = 12.5/13$ and side view in the vertical plane c) $\eta = 0$ and d) $\eta = \pi$ and e) $\eta = 2\pi/6$ and $\eta = 8\pi/6$. The black-lines plots were taken from Ozoe and Toh (1998) for comparison purposes.

Fig. 4 and Fig. 5 show the dynamics of the isotherms compared with the plots reported by Ozoe and Toh (1998) in the equivalent time of the simulation performed by the authors using another dimensional relationship.

IMPLI-C3 code can successfully recreates the problem using orthogonal collocation with Legendre polynomials. The central average can circumvent the singularity at the axial axis and demonstrate the advantage of the orthogonal collocation method, which increases the number of nodes in critical regions, such as near the boundaries.

3.3 Case III: Dynamics of natural convection in a differentially heated cubic cavity

The explanation of buoyancy-driven flow and heat transfer in a cubical cavity is a simple model problem of considerable practical interests as design of air-conditioning systems, storage of fruits and vegetables, food drying equipment, storage of cereal grains at silos, etc. The problem also provides an excellent test of numerical methods and computer codes used for the calculation of viscous convective flows. (De Vahl Davis, 1983; Bessonov *et al*., 1998; Tric *et al*., 2000; Wakashima and Saitoh, 2004; Ravnik *et al*., 2008; Brahim and Taieb, 2009; Lo *et al*., 2007).

The problem was analyzed using the Navier-Stokes equations in the form of velocity-vorticity (VV); this methodology removes the pressure term using curl to the momentum equation, and reduces expressions with vector properties to obtain a new variable denoted as vorticity.

Natural convection can analyze the transition effects between laminar and turbulent flow, with low viscosity fluids or higher temperature difference, that originate the development of important buoyancy effect that increases the fluid velocity, this buoyancy was modeled using Boussinesq approximation (Leonardi, 1984; Nield and Bejan, 1992).

Velocity-Vorticity Equations (VV):

$$\frac{\partial^2 U_x}{\partial X^2}+\frac{1}{\mathrm{A}_y{}^2}\frac{\partial^2 U_x}{\partial Y^2}+\frac{1}{\mathrm{A}_z{}^2}\frac{\partial^2 U_x}{\partial Z^2}=-\frac{1}{\mathrm{A}_y^2}\frac{\partial \omega_z}{\partial Y}+\frac{1}{\mathrm{A}_z^2}\frac{\partial \omega_y}{\partial Z} \tag{26a}$$

$$\frac{\partial^2 U_y}{\partial X^2}+\frac{1}{\mathrm{A}_y{}^2}\frac{\partial^2 U_y}{\partial Y^2}+\frac{1}{\mathrm{A}_z{}^2}\frac{\partial^2 U_y}{\partial Z^2}=\frac{\partial \omega_z}{\partial X}-\frac{1}{\mathrm{A}_z^2}\frac{\partial \omega_x}{\partial Z} \tag{26b}$$

$$\frac{\partial^2 U_z}{\partial X^2}+\frac{1}{\mathrm{A}_y{}^2}\frac{\partial^2 U_z}{\partial Y^2}+\frac{1}{\mathrm{A}_z{}^2}\frac{\partial^2 U_z}{\partial Z^2}=-\frac{\partial \omega_y}{\partial X}+\frac{1}{\mathrm{A}_y^2}\frac{\partial \omega_x}{\partial Y} \tag{26c}$$

Vorticity equations:

$$\frac{\partial \omega_x}{\partial \mathrm{Fo}}=-\left(\begin{array}{l} U_x\frac{\partial \omega_x}{\partial X}+U_y\frac{1}{\mathrm{A}_y{}^2}\frac{\partial \omega_x}{\partial Y}+U_z\frac{1}{\mathrm{A}_z{}^2}\frac{\partial \omega_x}{\partial Z} \\ -\omega_x\frac{\partial U_x}{\partial X}-\omega_y\frac{1}{\mathrm{A}_y{}^2}\frac{\partial U_x}{\partial Y}-\omega_z\frac{1}{\mathrm{A}_z{}^2}\frac{\partial U_x}{\partial Z}\end{array}\right)+\mathrm{Pr}\left(\frac{\partial^2 \omega_x}{\partial X^2}+\frac{1}{\mathrm{A}_y{}^2}\frac{\partial^2 \omega_x}{\partial Y^2}+\frac{1}{\mathrm{A}_z{}^2}\frac{\partial^2 \omega_x}{\partial Z^2}\right)+\mathrm{RaPr}\frac{\mathrm{A_z}}{\mathrm{A_y}{}^2}\frac{\partial \theta}{\partial Y} \tag{27a}$$

$$\frac{\partial \omega_y}{\partial \mathrm{Fo}}=-\left(\begin{array}{l} U_x\frac{\partial \omega_y}{\partial X}+U_y\frac{1}{\mathrm{A}_y{}^2}\frac{\partial \omega_y}{\partial Y}+U_z\frac{1}{\mathrm{A}_z{}^2}\frac{\partial \omega_y}{\partial Z} \\ -\omega_x\frac{\partial U_y}{\partial X}-\omega_y\frac{1}{\mathrm{A}_y{}^2}\frac{\partial U_y}{\partial Y}-\omega_z\frac{1}{\mathrm{A}_z{}^2}\frac{\partial U_y}{\partial Z}\end{array}\right)+\mathrm{Pr}\left(\frac{\partial^2 \omega_y}{\partial X^2}+\frac{1}{\mathrm{A}_y{}^2}\frac{\partial^2 \omega_y}{\partial Y^2}+\frac{1}{\mathrm{A}_z{}^2}\frac{\partial^2 \omega_y}{\partial Z^2}\right)-\mathrm{RaPrA_z}\frac{\partial \theta}{\partial X} \tag{27b}$$

$$\frac{\partial \omega_z}{\partial \mathrm{Fo}}=-\left(\begin{array}{l} U_x\frac{\partial \omega_z}{\partial X}+U_y\frac{1}{\mathrm{A}_y{}^2}\frac{\partial \omega_z}{\partial Y}+U_z\frac{1}{\mathrm{A}_z{}^2}\frac{\partial \omega_z}{\partial Z} \\ -\omega_x\frac{\partial U_z}{\partial X}-\omega_y\frac{1}{\mathrm{A}_y{}^2}\frac{\partial U_z}{\partial Y}-\omega_z\frac{1}{\mathrm{A}_z{}^2}\frac{\partial U_z}{\partial Z}\end{array}\right)+\mathrm{Pr}\left(\frac{\partial^2 \omega_z}{\partial X^2}+\frac{1}{\mathrm{A}_y{}^2}\frac{\partial^2 \omega_z}{\partial Y^2}+\frac{1}{\mathrm{A}_z{}^2}\frac{\partial^2 \omega_z}{\partial Z^2}\right) \tag{27c}$$

Energy balance:

$$\frac{\partial \theta}{\partial \mathrm{Fo}}=-\left(U_x\frac{\partial \theta}{\partial X}+\frac{U_y}{\mathrm{A}_y{}^2}\frac{\partial \theta}{\partial Y}+\frac{U_z}{\mathrm{A}_z{}^2}\frac{\partial \theta}{\partial Z}\right)+\left(\frac{\partial^2 \theta}{\partial X^2}+\frac{1}{\mathrm{A}_y{}^2}\frac{\partial^2 \theta}{\partial Y^2}+\frac{1}{\mathrm{A}_z{}^2}\frac{\partial^2 \theta}{\partial Z^2}\right) \tag{28}$$

Boundary conditions:

$$X=0, X=1, \quad U=0, \quad \omega_x=0, \quad \omega_y=-\frac{\partial U_z}{\partial X}, \quad \omega_z=\frac{\partial U_y}{\partial X}, \quad \theta=-0.5 \tag{29a}$$

$$Y=0, Y=1, \quad U=0, \quad \omega_x=\frac{\partial U_z}{\partial Y}, \quad \omega_y=0, \quad \omega_z=-\frac{\partial U_x}{\partial Y}, \quad \frac{\partial \theta}{\partial Y}=0 \tag{29b}$$

$$Z=0, Z=1, \quad U=0, \quad \omega_x=-\frac{\partial U_y}{\partial Z}, \quad \omega_y=\frac{\partial U_x}{\partial Z}, \quad \omega_z=0, \quad \frac{\partial \theta}{\partial Z}=0 \tag{29c}$$

All initial conditions start at zero.

The global Nusselt number represents the dimensionless rate of change of heat transfer across boundary in the hot wall (De Vahl Davis, 1983; Bessonov *et al*., 1998; Tric *et al*., 2000; Wakashima and Saitoh, 2004; Ravnik *et al*., 2008; Brahim and Taieb, 2009; Lo *et al*., 2007):

$$\mathrm{Nu} = \int_{-1/2}^{1/2}\int_{-1/2}^{1/2} \left.\frac{\partial(\mathrm{Y},\mathrm{Z})}{\partial \mathrm{X}}\right|_{X=1/2} dYdZ \qquad (30)$$

The simulations were performed for Pr =0.71, A_x=1, A_y=1, A_z=1, Ra = 10^3, 10^4, and 10^5 with a mesh of 11^3 and 17^3 internal nodes within a tolerance of 10^{-4}, carrying out the time integration to Fo = 0.5 using a relaxation factor of λ= 0.3 in the solution of the discretized equations. The results of the iterations and the Nusselt number are presented in Table 2.

Table 3 shows the comparison of the Nusselt number at different values of Ra. Table 4 details the maximum velocity compared to values obtained in previous experiments conducted by others authors. With a coarse grid, the values are in agreement with those reported with finer meshes. Also Fig. 6, shows the dynamics of the isotherms for Ra = 10^5 obtaining the well-known behavior of natural convection in the cubical cavity.

Table 2. Computational runs to verify the mesh independence of Case III

Ra	Mesh	Time increment (ΔFo)	Relaxation factor λ	Final Time (Fo)	Iterations	Nu
10^3	13×13×13	0.005	0.3	0.5	34009	1.0698
10^3	19×19×19	0.005	0.3	0.5	89249	1.0698
10^4	13×13×13	0.005	0.3	0.5	58420	2.0604
10^4	19×19×19	0.005	0.3	0.5	149990	2.0615
10^5	13×13×13	0.005	0.3	0.5	112791	4.4031
10^5	19×19×19	0.005	0.3	0.5	314255	4.3495

Table 3. Comparison of Nusselt number reported for the Case III

		Bessonov *et al*. (1998)	Tric *et al*. (2000)	Wakashima and Saitoh (2004)	Lo *et al*. (2007)	Ravnik *et al*. (2008)	Brahim and Taieb (2009)	This work
	Mesh	85×65×65	81^3	120^3	41^3	25^3	48^3	17^3
Nu	Ra=10^3	-	1.0700	-	1.0700	1.0713	1.07124	1.06979
	Ra=10^4	2.055	2.0542	2.0624	2.0540	2.0591	2.05604	2.06194
	Ra=10^5	4.339	4.3370	4.3665	4.3350	4.3570	4.34320	4.34951

Table 4. Comparison of Nusselt number and maximum velocity reported for Case III.

	Brahim and Taieb (2009)	Lo *et al*. (2007)	Tric *et al*. (2000)	This work
Mesh	48^3	41^3	81^3	17^3
		Ra=10^3		
Nu	1.07124	1.0710	1.0700	1.06979
U_{max}	3.53509	3.5227	3.54356	3.53007
V_{max}	0.17137	0.1726	0.17331	0.13516
W_{max}	3.54163	3.5163	3.54469	3.54415
		Ra=10^4		
Nu	2.05604	2.0537	2.0542	2.06194
U_{max}	16.68785	16.5312	16.71986	16.91797
V_{max}	2.15437	2.1092	2.15657	1.89773
W_{max}	18.96319	18.6971	18.98359	19.0026
		Ra=10^5		
Nu	4.34320	4.3329	4.3370	4.34951
U_{max}	43.84633	43.6877	43.9037	44.84974
V_{max}	9.63815	9.3720	9.6973	8.64359
W_{max}	71.02273	70.6267	71.0680	74.51753

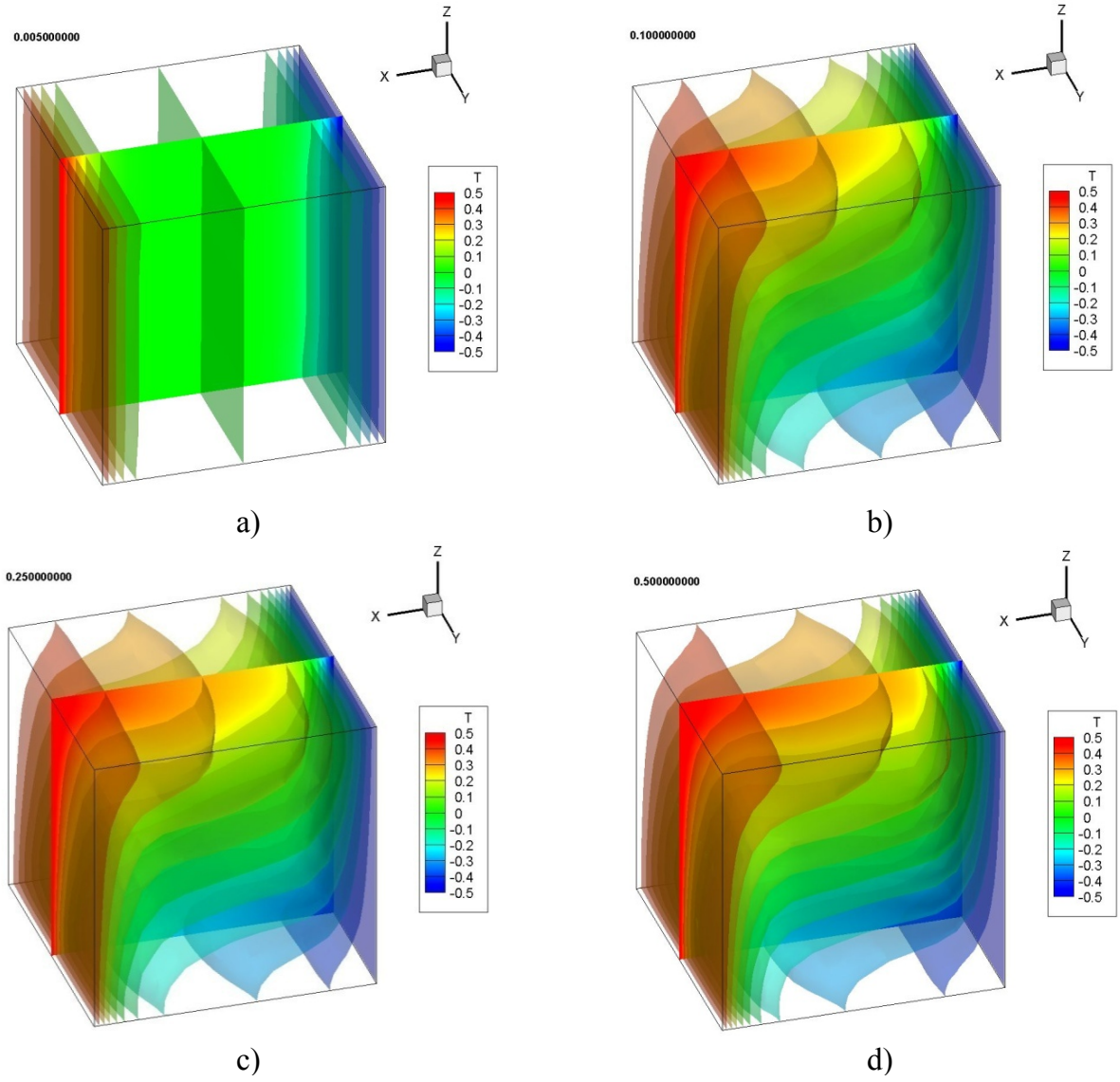

Fig. 6. Dynamic temperature isosurfaces for values of Ra=10^5 for: a) Fo = 0.005, b) Fo = 0.1, c) Fo = 0.25, and d) Fo = 0.5.

3.4 Case IV: Effect of temperature on natural convection in grain storage in cylindrical silos

Temperature and moisture are the most important factors that affect grain quality during storage at silos or bins. To improve these systems, it is needed accurate knowledge of the variation in temperature and moisture distribution during large periods. Temperature can be modified by both internal and external heat sources, changing the grain moisture equilibrium conditions in the cereal grain. Internal sources are related with grain respiration, insects and fungi proliferation, highly dependent of temperature and relative humidity of interstitial air. Instead, external sources are linked to environmental variation conditions in the storage period. Temperature gradients in the cereal grain favoring moisture migration from warmer to colder regions and this produce grain deterioration (Jimenez-Islas *et al.*, 2004; Abalone *et al.*, 2006; Balzi *et al.*, 2008). Given the economic importance of cereal grains production, the simulation techniques aid to achieve strategies to assess a safe storage in unventilated silos. The

numerical modeling is a useful tool to predict potential damage and provide storage conditions with particular environmental characteristics.

In this case, to obtain the mathematical model that governs the natural convection of heat and mass for grain storage in cylindrical silos, we considered a silo of radius R and height L that contains a Darcian, isotropic porous medium with interstitial spaces saturated with air. The intergranular air has an initial absolute humidity Y_0 (kg H_2O/kg dry air) and a dry-bulb temperature T_0. The bottom of the silo is insulated and the environmental temperature versus time is modeled via a fitted equation on the upper surface and lateral wall of the silo (Carrera-Rodríguez *et al*., 2011). In addition, the silo is impermeable, fluid flow is in laminar regime and ideal gas behavior.

The effect of the water activity of the grain (a_w), volumetric heat of respiration as a function of temperature, buoyancy effects due to temperature and concentration gradient (double diffusion effect) and latent heat of vaporization are all taken into account.

The equilibrium of humidity in the grain-air interface (Y_i) is defined as follows:

$$Y_i = \frac{18 {P_v}^0 a_w}{29(p - {P_v}^0 a_w)} \tag{31}$$

Where:

p = Atmospheric pressure

a_w = Water activity of the grain (calculated from the sorption isotherm)

P_v^0 = Vapor pressure for water (Jiménez-Islas *et al*., 2004).

To obtain the thermodynamic properties of cereal grains, sorghum was used as an example. The values in equations (16) to (19) were changed to those corresponding to the grain of interest. The data for the heat of respiration (Q_0) of sorghum reported by Mohsenin (1980) were adjusted using an exponential model by the least squares method yielding equation (17).

$$Q_0 = 1.837 \times 10^{-9} e^{(-6.5351 + 0.4604T - 0.006526T^2)} e^{87.804x} \tanh(0.00269x) \tag{32}$$

Where:

4.4 °C < T < 37.8 °C, 0.12 < x < 0.21, Q_0 = J/kg sorghum · s

x = Sorghum moisture in wet basis

$x = X/(X + 1)$

To calculate the generation of water (P_0) due the grain metabolism, the stoichiometry of the global reaction was used in correlation with the heat generation (Wilson, 1999). The calculations gave the following equation:

$$P_0 = 3.4118 \times 10^{-8} Q_0, \tag{33}$$

where P_0 is given in kg H_2O / kg sorghum · s. The sorption isotherm for the sorghum is as follows (Brooker *et al*., 1974):

$$a_w = 1 - \exp\left[-\exp\left(29.18 - 4.086\ln(T + 273.15) + 6.0346\ln x - 0.0105614(T + 273.15)\ln x\right)\right] \tag{34}$$

The vapor pressure of water according to the Antoine equation is as follows:

$$P_v^{\,0} = \exp\left(18.304 - \frac{3816.44}{T - 227.02}\right) \tag{35}$$

10 °C < T < 150 °C, P_v^0 [=] mm Hg.

Sorghum has a proximate composition on a dry basis of 11.82% protein, 80.57% carbohydrates, 3.52% lipids, 2.27% fiber, and 1.82 % ash (Woot-Tsuen and Flores, 1970); the sorghum grain has an average diameter of 0.003 m. The grain was stored in a small commercial cylindrical bin that was 1.33 m in radius and 2.76 m in height with a 15.3 m^3 grain capacity. The initial temperature of sorghum was 30 °C with 16% moisture (dry basis), while the environmental temperature was 25 °C with a relative humidity of 50% and an atmospheric pressure of 600 mm Hg. These conditions are typical in the Bajio, the agricultural region located in Guanajuato state, Mexico (Jiménez-Islas *et al*., 2004). Applying the methodology described in Case II, the governing equations are as follows:

Vector potential equations:

$$\omega_r = -\left(\frac{\partial^2\psi_r}{\partial\xi^2} + \frac{1}{\xi}\frac{\partial\psi_r}{\partial\xi} - \frac{\psi_r}{\xi^2} + \frac{1}{4\pi^2\xi^2}\frac{\partial^2\psi_r}{\partial\eta^2} - \frac{2}{4\pi^2\xi^2}\frac{\partial\psi_\theta}{\partial\eta} + \frac{1}{A^2}\frac{\partial^2\psi_r}{\partial\zeta^2}\right) \tag{36a}$$

$$\omega_\theta = -\left(\frac{\partial^2\psi_\theta}{\partial\xi^2} + \frac{1}{\xi}\frac{\partial\psi_\theta}{\partial\xi} - \frac{\psi_\theta}{\xi^2} + \frac{1}{4\pi^2\xi^2}\frac{\partial^2\psi_\theta}{\partial\eta^2} + \frac{2}{\xi^2}\frac{\partial\psi_r}{\partial\eta} + \frac{1}{A^2}\frac{\partial^2\psi_\theta}{\partial\zeta^2}\right) \tag{36b}$$

$$\omega_z = -\left(\frac{\partial^2\psi_z}{\partial\xi^2} + \frac{1}{\xi}\frac{\partial\psi_z}{\partial\xi} + \frac{1}{4\pi^2\xi^2}\frac{\partial^2\psi_z}{\partial\eta^2} + \frac{1}{A^2}\frac{\partial^2\psi_z}{\partial\zeta^2}\right) \tag{36c}$$

Vorticity equations:

$$\frac{\partial \omega_r}{\partial \mathrm{Fo}} = -\frac{\mathrm{Pr}}{\mathrm{Da}}\omega_r + \mathrm{Pr}\left(\frac{\partial^2\omega_r}{\partial\xi^2} + \frac{1}{\xi}\frac{\partial\omega_r}{\partial\xi} - \frac{\omega_r}{\xi^2} + \frac{1}{4\pi^2\xi^2}\frac{\partial^2\omega_r}{\partial\eta^2} - \frac{2}{4\pi^2\xi^2}\frac{\partial\omega_\theta}{\partial\eta} + \frac{1}{\mathrm{A}^2}\frac{\partial^2\omega_r}{\partial\zeta^2}\right) + \mathrm{RaPrA}\left[\frac{1}{4\pi^2\xi}\frac{\partial\theta}{\partial\eta} + \frac{\mathrm{N}}{4\pi^2\xi}\frac{\partial\phi}{\partial\eta}\right] \tag{36d}$$

$$\frac{\partial \omega_\theta}{\partial \mathrm{Fo}} = -\frac{\mathrm{Pr}}{\mathrm{Da}}\omega_\theta + \mathrm{Pr}\left(\frac{\partial^2\omega_\theta}{\partial\xi^2} + \frac{1}{\xi}\frac{\partial\omega_\theta}{\partial\xi} - \frac{\omega_\theta}{\xi^2} + \frac{1}{4\pi^2\xi^2}\frac{\partial^2\omega_\theta}{\partial\eta^2} + \frac{2}{\xi^2}\frac{\partial\omega_r}{\partial\eta} + \frac{1}{\mathrm{A}^2}\frac{\partial^2\omega_\theta}{\partial\zeta^2}\right) - \mathrm{RaPrA}\left[\frac{\partial\theta}{\partial\xi} + \mathrm{N}\frac{\partial\phi}{\partial\xi}\right] \tag{36e}$$

$$\frac{\partial \omega_z}{\partial \mathrm{Fo}} = -\frac{\mathrm{Pr}}{\mathrm{Da}}\omega_z + \mathrm{Pr}\left(\frac{\partial^2\omega_z}{\partial\xi^2} + \frac{1}{\xi}\frac{\partial\omega_z}{\partial\xi} + \frac{1}{4\pi^2\xi^2}\frac{\partial^2\omega_z}{\partial\eta^2} + \frac{1}{\mathrm{A}^2}\frac{\partial^2\omega_z}{\partial\zeta^2}\right) \tag{36f}$$

Energy balance:

$$\begin{aligned}\frac{\partial\theta}{\partial\mathrm{Fo}} = &-\left[\left(\tfrac{1}{4\pi^2\xi}\tfrac{\partial\psi_z}{\partial\eta} - \tfrac{1}{\mathrm{A}^2}\tfrac{\partial\psi_\theta}{\partial\zeta}\right)\tfrac{\partial\theta}{\partial\xi} + \tfrac{1}{4\pi^2\xi}\left(-\tfrac{\partial\psi_z}{\partial\xi} + \tfrac{1}{\mathrm{A}^2}\tfrac{\partial\psi_r}{\partial\zeta}\right)\tfrac{\partial\theta}{\partial\eta} + \tfrac{1}{\mathrm{A}^2}\left(\tfrac{\partial\psi_\theta}{\partial\xi} + \tfrac{\psi_\theta}{\xi} - \tfrac{1}{4\pi^2\xi}\tfrac{\partial\psi_r}{\partial\eta}\right)\tfrac{\partial\theta}{\partial\zeta}\right] \\ &+\tfrac{\partial^2\theta}{\partial\xi^2} + \tfrac{1}{\xi}\tfrac{\partial\theta}{\partial\xi} + \tfrac{1}{4\pi^2\xi^2}\tfrac{\partial^2\theta}{\partial\eta^2} + \tfrac{1}{\mathrm{A}^2}\tfrac{\partial^2\theta}{\partial\zeta^2} + \tfrac{Q_0\rho_s R^2}{(T_1-T_0)k_{eff}} - \tfrac{\lambda_v k_y a_v \rho_a (Y_i - [Y_0+\phi_a(Y_1-Y_0)])R^2}{(T_1-T_0)k_{eff}}\end{aligned} \tag{36g}$$

Grain moisture balance:

$$\frac{\partial\phi_s}{\partial\mathrm{Fo}} = \frac{1}{\mathrm{Le_s}}\left(\frac{\partial^2\phi_s}{\partial\xi^2} + \frac{1}{\xi}\frac{\partial\phi_s}{\partial\xi} + \frac{1}{4\pi^2\xi^2}\frac{\partial^2\phi_s}{\partial\eta^2} + \frac{1}{\mathrm{A}^2}\frac{\partial^2\phi_s}{\partial\zeta^2}\right) + \frac{P_0\rho_s R^2}{\rho_s\alpha(X_1-X_0)} - \frac{k_y a_v \rho_a (Y_i - [Y_0+\phi_a(Y_1-Y_0)])R^2}{\rho_s\alpha(X_1-X_0)} \tag{36h}$$

Air humidity balance:

$$\begin{aligned}\frac{\partial\phi_a}{\partial\mathrm{Fo}} = &-\left[\left(\tfrac{1}{4\pi^2\xi}\tfrac{\partial\psi_z}{\partial\eta} - \tfrac{1}{\mathrm{A}^2}\tfrac{\partial\psi_\theta}{\partial\zeta}\right)\tfrac{\partial\phi_a}{\partial\xi} + \tfrac{1}{4\pi^2\xi}\left(-\tfrac{\partial\psi_z}{\partial\xi} + \tfrac{1}{\mathrm{A}^2}\tfrac{\partial\psi_r}{\partial\zeta}\right)\tfrac{\partial\phi_a}{\partial\eta} + \tfrac{1}{\mathrm{A}^2}\left(\tfrac{\partial\psi_\theta}{\partial\xi} + \tfrac{\psi_\theta}{\xi} - \tfrac{1}{4\pi^2\xi}\tfrac{\partial\psi_r}{\partial\eta}\right)\tfrac{\partial\phi_a}{\partial\zeta}\right] \\ &+\tfrac{1}{\mathrm{Le}_a}\left(\tfrac{\partial^2\phi_a}{\partial\xi^2} + \tfrac{1}{\xi}\tfrac{\partial\phi_a}{\partial\xi} + \tfrac{1}{4\pi^2\xi^2}\tfrac{\partial^2\phi_a}{\partial\eta^2} + \tfrac{1}{A^2}\tfrac{\partial^2\phi_a}{\partial\zeta^2}\right) + \tfrac{k_y a_v (Y_i - Y)R^2}{\alpha(Y_1-Y_0)}\end{aligned} \tag{36i}$$

The Lewis number (Le) represent the ratio between thermal and mass diffusivities, is a thickness measurement of thermal and concentration layer, representing the heat ability to be transported by diffusion. The energy balance has two production terms, the volumetric heat of respiration in the grain and the loss heat due moisture vaporization. The grain moisture balance has a term representing the volumetric velocity by humidity generation due cereal grain respiration and the water transferred to the air. The air humidity balance has a term that represents the moisture gain by the water release by the cereal grain.

Temperature boundary conditions for this silo consist of an insulated base, and the surroundings are affected by environmental temperature predicted by the following equations reported by Carrera-Rodríguez *et al*. (2011).

$$\theta = \frac{\left[\frac{T_1+T_2}{2} + T_1 - \frac{T_1+T_2}{2}\cos\left[\left(\frac{4.5}{16}\right)\left(\frac{FoR^2}{3600\alpha}\right) - \frac{16T_2}{T_1}\right]\right] - T_0}{T_f - T_0} \tag{37}$$

Where

$$T_1 = T_{\max}\exp\frac{-\left[\left(\frac{\mathrm{Fo}\,R^2}{86400\alpha}\right) - 159.823\right]^2}{2(245.07)^2} \tag{38a}$$

$$T_2 = T_m\exp\frac{-\left[\left(\frac{\mathrm{Fo}\,R^2}{86400\alpha}\right) - 190.767\right]^2}{2(131.334)^2} \tag{38b}$$

Equations (22a-c) involve both day-night and seasonal cycles, therefore, they have the ability to predict the ambient temperature over a year (January 1 to December 31). The variables required for the calculation in the year 2009 in the state of Guanajuato, Mexico are presented in Table 5 and equations (22a-c) are adapt easily to predict environmental temperature in other localities (Carrera-Rodriguez *et al*., 2011). Mass boundary conditions assumed an impermeable silo; therefore, the moisture interchanging between silo and ambience is negligible. Hence, the boundary conditions are as follows:

$$\xi = 0, \quad Average, \quad Average, \quad Average, \quad Average \tag{39a}$$

$$\xi = 1, \quad \begin{matrix} \frac{\partial \psi_r}{\partial \xi} = 0 \\ \psi_\theta = 0 \psi_z = 0 \end{matrix}, \theta = f(\text{Fo}), \frac{\partial W}{\partial \xi} = 0, \frac{\partial \varphi}{\partial \xi} = 0 \tag{39b}$$

$$\eta = 0, \quad \frac{\partial \psi_0}{\partial \eta} = \frac{\partial \psi_n}{\partial \eta}, \frac{\partial \theta_0}{\partial \eta} = \frac{\partial \theta_n}{\partial \eta}, \quad \frac{\partial W_0}{\partial \eta} = \frac{\partial W_n}{\partial \eta}, \frac{\partial \phi_0}{\partial \eta} = \frac{\partial \phi_n}{\partial \eta} \tag{39c}$$

$$\eta = 1, \quad \psi_0 = \psi_n, \theta_0 = \theta_n, W_0 = W_n, \phi_0 = \phi_n \tag{39d}$$

$$\zeta = 0, \quad \begin{matrix} \psi_r = 0 \\ \psi_\theta = 0 \\ \frac{\partial \psi_z}{\partial \zeta} = 0 \end{matrix}, \frac{\partial \theta}{\partial \zeta} = 0, \frac{\partial W}{\partial \zeta} = 0, \frac{\partial \phi}{\partial \zeta} = 0 \tag{39e}$$

$$\zeta = 1, \quad \begin{matrix} \psi_r = 0 \\ \psi_\theta = 0 \\ \frac{\partial \psi_z}{\partial \zeta} = 0 \end{matrix}, \theta = f(\text{Fo}), \frac{\partial W}{\partial \zeta} = 0, \frac{\partial \phi}{\partial \zeta} = 0 \tag{39f}$$

Wood's approximation was used for the vorticity boundaries (Leonardi, 1984). The initial conditions are as follows:

$$Fo = 0, \quad \psi = 0, \quad \theta = 0, \quad W = 0, \quad \phi = 0 \tag{40}$$

Fig. 7 shows the geometric system and computational domain, including the radial and axial coordinates, with a grid of 9×18×9 collocation points yielding 21,780 algebraic equations, and a time-step size of 10^{-4} performing the simulation until one day of real time (January 1). Due to the stiffness of the governing equations, a relaxation factor $\lambda = 0.3$ was used. The system reached convergence in 12,424,325 iterations with a CPU time of 7 days. This CPU time can be reduced substantially if one uses parallelization computing in workstations or supercomputers. In addition, the hardware, the operating systems and the FORTRAN compilers are becoming more efficient. Fig. 8 shows the flow patterns and temperature contours, the solid lines in black represent the path of the air inside the silo and the color contours represented temperatures. At Fo = 0, the dynamic temperature inside the silo is homogenous. There is an increase in the temperature in the silo (approximately 10:00 h). This rise of the surrounding environmental temperature accelerates the respiration heat source leading to an increase in the temperature inside the silo. During the warmest hours of the day (approximately 12:00 h to 14:00 h), temperature gradients concentrate on the sidewall and the surface of grains. Similarly, when a cold cycle arrives, the temperature decreases at the boundary due to the effect of environmental boundary conditions as reported by Balzi *et al*. (2008). The dynamic central part is the least sensitive to environmental changes. These results are consistent with those reported by Abalone *et al*. (2006) and Carrera-Rodríguez *et al*. (2011). Flow patterns show a recirculation near the boundaries of cold air moving down the borders causing the bottom to cool faster. The flow patterns spread across the silo, and when the temperature cycle begins again, cold flow patterns re-form near the borders, validating the model proposed by Carrera-Rodríguez *et al*. (2011).

Table 5. Representative temperature values of the state of Guanajuato, Mexico for 2009.

Variable	°C	Description
T_{max}	30.7	Annual maximum temperature
T_{min}	4.9	Annual minimum temperature
T_m	14.9	Maximum temperature, minimum annual
T_o	30.0	Initial grain temperature
T_f	25.0	Initial temperature of the environment

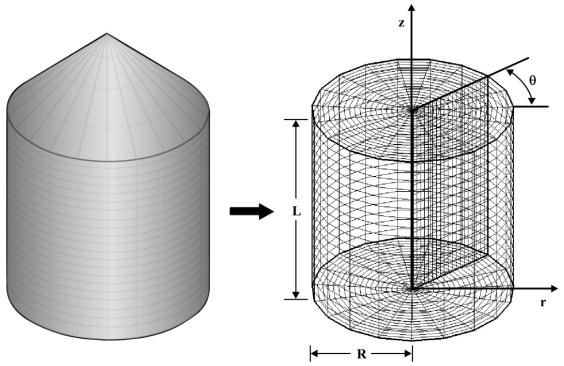

Fig. 7. Three-dimensional computational domain for Case IV.

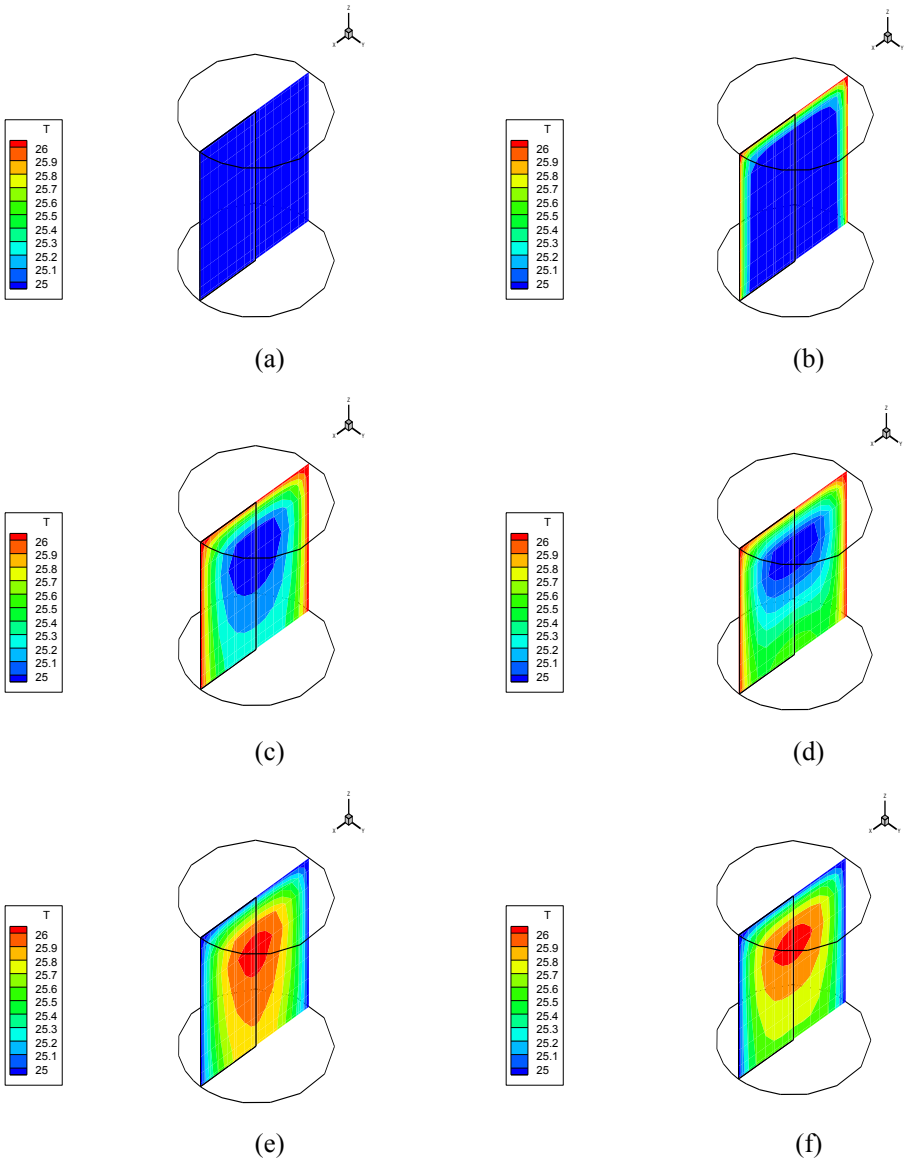

Fig. 8. Temperature contours for January 1 for: a) 00:00 h, b) 10:00 h, c) 12:00 h, d) 16:00 h, e) 18:00 h, and f) 20:00 h.

Table 6. Use of computer memory for a defined mesh for the different problems analyzed.

	Mesh	Nonlinear equations	NEWIMP-C3 Memory (Kb)	IMPLI-C3 Memory (Kb)
Case I	50×50×50	281,216	1,289,156	18,996
Case II	10×25×10	27,216	1,597,776	4,996
Case III	20×20×20	74,536	1,468,280	7,600
Case IV	21×23×21	119,025	1,638,072	10,028

3.5 Memory use

We also performed a RAM memory study to illustrate advantages of nonlinear relaxation versus classic Newton-Raphson multivariate, designing a Newton-Raphson computer code with similar subroutines and operational characteristics of IMPLI-C3. This code was named NEWIMP-C3 and his utilization will be reported later. The comparison was performed with the same type of discretization and an equal amount of free memory, the different cases was carried out with meshing close to use all free memory available, depending on the problem, comparing the RAM consumption. Table 6 shows the assigned memory showed in the Windows^{TM} Task Manager, the large difference between memory consumption illustrates that nonlinear relaxation has a great advantage to save memory and allowing address complex problems that require large amount of nodes for enhancing the accuracy of solution. We also observed that memory consumption by nonlinear relaxation is only 0.3%-1.5% of the memory required by Newton-Raphson, so the nonlinear relaxation is a robust algorithm that allows simulating complex problems that require large number of nodes.

Conclusions

The IMPLI-C3 FORTRAN code was suitable to solve problems involving 3-D parabolic nonlinear PDE, particularly in the natural convection simulations, decreasing substantially the amount of required RAM (approximately 1 % of the memory required if one uses Newton-Raphson), without any complex algebraic-rearrangement of governing equations. This allows the implementation of finer meshes that are required in numerical analysis of complex highly nonlinear problems, where the Newton method is unfeasible due the amount of memory required that often exceed the installed RAM. The use of 3-D orthogonal collocation for discretizing spatial coordinates is an alternative methodology for solving engineering problems with accuracy.

Acknowledgments

We gratefully acknowledge the financial support of CONACYT, Mexico via grants Basic Science SEP-2004-CO1-46230 and CB-2011/167095, and CONCYTEG (Guanajuato State Government) via grants 07-09-k662-050, 07-09-k119-107, and 09-09-k662-065.

Nomenclature

A	ratio height/radius, L/R
a_v	grain-air interfacial area, $m^2\ m^{-3}$
a_w	water activity, dimensionless
e	unit vector
C	matrix used for the calculation of the matrix A
D	matrix used for the calculation of the matrix B
F	function
Fo	Fourier number
Nu	Nusselt number
NX	number of internal nodes in X direction
NY	number of internal nodes in Y direction
NZ	number of internal nodes in Z direction
P	polynomial
P	pressure
P_0	volumetric generation of water by respiration, $kg\ m^{-3}\ s^{-1}$
Pr	Prandtl number
Q	matrix used for the calculation of the matrices A and B
Q_0	volumetric heat of respiration of the cereal grain, $J^{-3}\ s^{-1}$
R	cylinder radius
Ra	Rayleigh number
T	dependent variable, temperature
T	independent variable matrix
U	dimensionless velocity
X, x	spatial coordinate in X direction
Y, y	spatial coordinate in Y direction
Z, z	spatial coordinate in Z direction
X	grain moisture in dry basis, kg water/kg dry solid
Y_i	absolute humidity in the grain-air interface, kg water/kg dry air
Y	absolute humidity, kg water/kg dry air

Subscripts

J	local index node X
I	local node index in Y
k, p	auxiliary indexes
N	number of internal nodes
0, 1	initial, final condition

Greek symbols

α	thermal diffusivity of the porous medium, $k_{eff}/\rho C_p$
ω	vorticity

ψ vector potential
θ temperature
λ relaxation factor
ξ dimensionless radial coordinate, r/R
ϕ_s dimensionless moisture grain, $(X - X_0)/(X_1 - X_0)$
ϕ_a dimensionless humidity in the air, $(Y - Y_0)/(Y_1 - Y_0)$
ζ dimensionless height coordinate, z/L
η dimensionless angular or azimuthal coordinate, $\theta/2\pi$
ρ density, kg/m^3
ρ_a density of dry air, kg/m^3
ρ_s sorghum grain density on dry basis, kg/m^3

References

Abalone, R., Gastón, A., Cassinera, A. and Lara, M. A. (2006). Modelización de la Distribución de Temperatura y Humedad de Granos Almacenados en Silos. *Asociación Argentina de Mecánica Computacional. Mecánica Computacional*; 233-247.

Balzi, U. R., Gastón, A., and Abalone, R. (2008). Efecto de la Convección Natural en la Distribución de Temperatura y Migración de Humedad en Granos Almacenados en Silos. *Asociación Argentina de Mecánica Computacional. Mecánica Computacional*, 1471-1485.

Barrozo, M. A. S., Henrique, H. M., Sartori, D. J. M. and Freire, J. T. (2006). The use of the orthogonal collocation method on the study of the drying kinetics of soybean seeds. *Journal of Stored Products Research 42*, 348-356.

Bessonov, O. A., Brailovskaya, V.A., Nikitin, S.A., and Polezhaev, V. I. (1998). Three-Dimensional Natural Convection in a Cubical Enclosure: A Benchmark Numerical Solution. *Advances in Computational Heat Transfer Procedures of International Symposium Cesme*, 1.

Brahim, B. B. and Taieb, L. (2009). Transient natural convection in 3D tilted enclosure heated from two opposite sides. *International Communications in Heat and Mass Transfer 36*, 604-613.

Brooker, D. B., Bakker-Arkema, F. W. and Hall C. W. (1974). *Drying Cereal Grains*. AVI Publishing Company: Westport, Connecticut. USA.

Carrera-Rodríguez, M., Martínez-González, G. M., Navarrete-Bolaños, J. L., Botello-Álvarez, J. E., Rico-Martínez, R. and Jiménez-Islas, H. (2011). Transient numerical study of the effect of ambient temperature on 2-D cereal grain storage in cylindrical silos. *Journal of Stored Products Research 47*, 106-122.

De Vahl, Davis, G. (1983). Natural Convection of Air in a Square Cavity: A Benchmark Numerical Solution. *International Journal for Numerical Methods in Fluids 3*, 249-264.

Ebrahimi, A. A., Ebrahim, H. A. and Jamshidi, E. (2008). Solving partial differential equations of gas-solid reactions by orthogonal collocation. *Computers & Chemical Engineering 32*, 1746-1759.

Finlayson, B. A. (1972). *The Method of Weighted Residuals and Variational Principles*, Academic Press. USA.

Finlayson, B. A. (1980). *Nonlinear Analysis in Chemical Engineering*. McGraw-Hill College. USA

Jiménez-Islas, H. and López-Isunza, F. (1994). ELI-COL Programa para resolver sistemas de ecuaciones diferenciales parciales elípticas, por doble colocación ortogonal. *Avances en Ingeniería Química 2*, 82-86.

Jiménez-Islas H. and López-Isunza F. (1996). PAR-COL2, Programa para resolver EDP parabólicas bidimensionales no lineales, por doble colocación ortogonal. *Avances en Ingeniería Química 4*, 168-173.

Jiménez-Islas, H. (1999). *Modelamiento Matemático de los Procesos de Transferencia de Momentum, Calor y Masa en Medios Porosos*. PhD Thesis (in Spanish), Universidad Autónoma Metropolitana Unidad Iztapalapa, México, D.F.

Jiménez-Islas, H., Navarrete-Bolaños, J. L. and Botello-Álvarez, E. (2004). Numerical Study of the Natural Convection of Heat and 2-D Mass of Grain Stored in Cylindrical Silos. *Agrociencia 38*, 325-342

Jiménez-Islas, H. (2001). Natural Convection in a Cubical Porous Cavity: Solution by Orthogonal Collocation. Computational Fluid Dynamics; *Proceedings of the Fourth UNAM Supercomputing Conference. World Scientific Publishing Co. Singapore*, 173-180.

Leonardi, E. A. (1984). *Numerical Study of the Effects of Fluid Properties on Natural Convection*. Ph.D. Thesis. University of New South Wales, Australia.

Lo, D. C., Young, D. L., Murugesan, K., Tsai, C. C., and Gou, M. H. (2007). Velocity-Vorticity formulation for 3D natural convection in an inclined cavity by DQ method. *International Journal of Heat and Mass Transfer 50*, 479-491.

Mohsenin, N. N. (1980). *Thermal Properties of Foods and Agricultural Materials* (2nd ed. pp 407). Gordon and Breach Science Publishers: NY. USA.

Nield, D. A. and Bejan, A. (1992). *Convection in Porous Media*. Springer-Verlag, USA.

Ostrach, S. (1988). Natural Convection in Enclosures. *Journal of Heat Transfer 110*, 1175-1190

Ozoe, H. and Toh, K. A. (1998). Technique to circumvent a singularity at a radial center with application for a three-dimensional cylindrical system. Numerical Heat Transfer, Part B. Fundamentals. *An International Journal of Computation and Methodology 33*, 355-365.

Ravnik, J., Skerget, L. and Zunic, Z. (2008). Velocity-Vorticity formulation for 3-D natural convection in an inclined enclosure by FEM. *International Journal of Heat and Mass Transfer 51*, 4517-4527.

Roache, P.J. (1972). *Computational Fluid Dynamics*. Hermosa Publisher: Albuquerque, N.M. USA.

Tric, E., Labrose, G. and Betrouni, M. (2000). A first incursion into the 3D structure of natural convection of air in a differentially heated cubic cavity from accurate numerical solutions. *International Journal of Heat and Mass Transfer 43*, 4043-4056.

Vemuri, V. R. and Karplus, W. J. (1981). *Digital Computer Treatment of Partial Differential Equations*. Prentice-Hall Co. USA.

Villadsen, J. V. and Stewart, W. E. (1967). Solution of Boundary-Value Problems by Orthogonal Collocation. *Chemical Engineering Science 22*, 1483-1501.

Wakashima, S. and Saitoh, T. S. (2004). Benchmark solutions for natural convection in a cubic cavity using the high-order time-space method. *International Journal of Heat and Mass Transfer 47*, 853-864.

Wilson, M. T. (1999). A Model for Predicting Mould Growth and Subsequent heat Generation in Bulk Stored Grain. *Journal of Stored Products Research 35*, 1-13.

Woot-Tsuen, W. and Flores, M. (1970). *Tabla de Composición de Alimentos para uso en América Latina* (pp 150). Editorial Interamericana, S.A., México.